JGR Oceans

RESEARCH ARTICLE
10.1029/2026JC024472

Key Points:

- Coral $\delta^{18}O$ reveals decadal variability of TC precipitation from 1906 to 2012 CE
- Atlantic Multidecadal Oscillation and solar forcing dominate the low-frequency variability of TC precipitation in the Northwest Pacific
- The impacts of ENSO and Pacific Decadal Oscillation on TC precipitation in the Northwest Pacific vary across different periods

Supporting Information:

Supporting Information may be found in the online version of this article.

Correspondence to:

W. Jiang,
jianwe@gxu.edu.cn

Citation:

Shi, Y., Jiang, W., Yong, Y., Gu, T., Liu, C., Du, S., et al. (2026). Atlantic Multidecadal Oscillation and Solar forcing modulate decadal-scale variability in Northwest Pacific tropical cyclone precipitation. *Journal of Geophysical Research: Oceans*, *131*, e2026JC024472. https://doi.org/10.1029/2026JC024472

Received 21 APR 2026
Accepted 13 SEP 2026

Author Contributions:

Conceptualization: Wei Jiang
Data curation: Yuchen Shi, Wei Jiang
Formal analysis: Yuchen Shi, Wei Jiang
Funding acquisition: Kefu Yu
Investigation: Yuchen Shi
Methodology: Yuchen Shi, Wei Jiang
Project administration: Wei Jiang, Kefu Yu
Resources: Wei Jiang
Software: Yuchen Shi
Supervision: Wei Jiang, Kefu Yu
Validation: Yuchen Shi, Wei Jiang
Visualization: Wei Jiang
Writing – original draft: Yuchen Shi
Writing – review & editing: Wei Jiang, Yangyang Yong, Tingwu Gu, Caifeng Liu, Siqi Du, Yuyan Jiang, Ting Yang, Hui Ouyang

© 2026 American Geophysical Union. All rights reserved, including rights for text and data mining and training of artificial intelligence technologies or similar technologies.

Atlantic Multidecadal Oscillation and Solar Forcing Modulate Decadal-Scale Variability in Northwest Pacific Tropical Cyclone Precipitation

Yuchen Shi[1], Wei Jiang[2,3], Yangyang Yong[2,3], Tingwu Gu[2,3], Caifeng Liu[2,3], Siqi Du[2,3], Yuyan Jiang[1], Ting Yang[2,3], Hui Ouyang[1], and Kefu Yu[2,3,4]

[1]School of Resources, Environment and Materials, Guangxi University, Nanning, China, [2]Guangxi Laboratory on the Study of Coral Reefs in the South China Sea, Guangxi University, Nanning, China, [3]School of Marine Sciences, Guangxi University, Nanning, China, [4]Southern Marine Sciences and Engineering Guangdong Laboratory (Guangzhou), Guangzhou, China

Abstract Extreme precipitation associated with tropical cyclones (TCs) poses a growing threat to coastal communities, yet short instrumental records hamper the assessment of long-term variability. Here, we address this gap by developing a quantitative proxy for TC precipitation using a previously published, monthly resolved coral oxygen isotope ($\delta^{18}O$) record. This record was derived from a single *Porites* coral specimen collected offshore southern Taiwan, a region within the most active TC zone of the Northwest Pacific. Because coral $\delta^{18}O$ reflects both sea surface temperature and seawater $\delta^{18}O$, we infer TC precipitation from the hydrological and isotopic imprint of isotopically depleted freshwater input recorded by the coral. Calibrated against modern data (1998–2012 CE), the proxy identified extreme TC events with a detection rate of ~78%. We reconstructed a coral-based index of TC precipitation variability for 1906–2012 CE. We then characterized the low-frequency variability of the reconstructed index using spectral analysis and evaluated its associations with major climate drivers using correlation analyses. The 106-year record revealed pronounced interdecadal variability primarily modulated by the Atlantic Multidecadal Oscillation and solar forcing, while the influences of El Niño–Southern Oscillation and Pacific Decadal Oscillation were non-stationary, becoming more coherent after the 1950s. Our reconstruction constrains pre-instrumental TC hydroclimate variability and its drivers, informing future projections and coastal risk assessment under continued warming.

Plain Language Summary Extreme rainfall from tropical cyclones poses a growing threat to coastal communities, but short weather records make it difficult to know how tropical cyclone (TC) activity has varied over long timescales. In this study, we developed a new way to detect past TC rainfall using a previously published oxygen isotope record from a single coral specimen collected offshore southern Taiwan, a region located in the Northwest Pacific's most active TC zone. By comparing the modern portion of this coral record with instrumental observations from 1998 to 2012 CE, we found that our coral-based method correctly identifies about 78% of extreme TC rainfall events. We then applied this method to reconstruct a coral-based index of TC precipitation variability from 1906 to 2012 CE. The century-long record shows that TC rainfall activity varied naturally over decades, primarily driven by the Atlantic Multidecadal Oscillation and changes in solar output. Interestingly, the influences of El Niño–Southern Oscillation and Pacific Decadal Oscillation were weak before the 1950s but became stronger afterward. By extending the observational baseline back more than a century, our reconstruction helps scientists better understand the natural drivers of TC rainfall and improves our ability to assess future coastal risks under continued warming.

1. Introduction

In a warming climate, the frequency and intensity of extreme weather events have increased markedly (Shan et al., 2023; X. M. Shi et al., 2024). TCs are among the most destructive of these phenomena, bringing hazardous winds, intense precipitation, and storm surges that pose severe threats to coastal communities and ecosystems (Gori et al., 2022; Hu et al., 2023; Kropf et al., 2025). Recent studies have reported a significant increase in the intensity of extreme precipitation events during TC seasons (Chu et al., 2018; Henny et al., 2021). Compared with historical levels, TC-associated extreme precipitation has become substantially more destructive (Qi et al., 2025; Qin et al., 2024). Observations further indicate a significant rise in the occurrence of rapidly intensifying TCs over the past four decades (Bhatia et al., 2022). Whether these changes reflect a direct response to anthropogenic

warming or arise from natural multidecadal variability remains a central scientific question (Lin et al., 2025; S. Wang et al., 2023; W. Zhou et al., 2025). Resolving this uncertainty is critical for projecting future TC risks and for guiding climate adaptation in vulnerable regions (Jullien et al., 2024; Kropf et al., 2025).

The understanding of TC variability, based on the observational data in the Northwest Pacific—the most active TC basin on Earth, emphasizes its modulation by major climate modes operating across different timescales. Trans-basin teleconnections from the Atlantic Multidecadal Oscillation (AMO) are recognized as a key driver of low-frequency changes in Northwest Pacific TC activity, primarily through modifications of regional sea surface temperatures and atmospheric circulation (Cao et al., 2025; H. P. Huang et al., 2023; K. X. Song et al., 2024; C. Sun et al., 2020; J. W. Zhao et al., 2024). External forcing from solar variability has also been implicated in TC variability, potentially through impacts on radiative balance and atmospheric structure (Huo et al., 2021; Huo et al., 2023; S. Li, Li, & Ling, 2023). In addition, the El Niño–Southern Oscillation (ENSO) and the Pacific Decadal Oscillation (PDO) are established dominant controls on interannual-to-decadal variations in TC tracks, intensity, and genesis frequency across the basin (C. Huang et al., 2022; Mueller et al., 2024; Scoccimarro et al., 2021; Shi et al., 2025; H. K. Zhao & Wang, 2019; C. Zhou et al., 2024). However, their contributions to the long-term, low-frequency variability of TC precipitation remain poorly quantified, especially during the pre-instrumental period. Resolving the relative contributions of these internal and external forcings to decadal-scale TC precipitation variability is therefore critical for advancing attribution of recent trends and for refining future projections in a warming climate.

Owing to the limited temporal coverage of instrumental records, the detection and attribution of decadal-scale variability in TC activity remain challenging (Emanuel, 2021; Minamidate & Goto, 2024). This gap has driven the emergence of paleotempestology, which seeks to reconstruct long-term TC histories using geological and biological proxy archives (Monica et al., 2024; Thoppil, 2025; Yang et al., 2024; N. Y. Zhao et al., 2025). Despite their widespread application in paleotempestology, sedimentary archives, tree-ring records, and speleothems are often constrained by insufficient temporal resolution and chronological uncertainty, limiting their capacity to resolve short-duration TC events (Altman et al., 2021; L. Chen et al., 2024; Donnelly, 2025; Frappier, 2013; Wallace et al., 2024; Y. S. Wu et al., 2019). By comparison, massive corals such as *Porites* grow continuously in nearshore environments, providing well-dated, monthly resolved geochemical records of ambient seawater conditions (Han et al., 2024; Kench et al., 2025; Tao et al., 2024). Critically, the oxygen isotope composition ($\delta^{18}O$) of coral skeletons is sensitive to the meteoric freshwater input from heavy TC precipitation which is characterized by markedly lower $\delta^{18}O$ values than those associated with monsoonal or typical convective precipitation, owing to intensified isotopic fractionation during TC systems (F. J. Chen et al., 2021; Jackisch et al., 2022; C. J. Sun et al., 2022). This isotopic depletion provides a mechanistic basis for using the coral $\delta^{18}O$ record to identify TC precipitation signals at high temporal resolution.

This study uses a previously published, high-resolution coral $\delta^{18}O$ record derived from a single *Porites* specimen collected offshore southern Taiwan to examine TC precipitation in the region (Ramos et al., 2020). The study area is located within one of the most active TC zones of the Northwest Pacific, where instrumental observations indicate that TC precipitation has increased dramatically since the late 1990s. Extreme precipitation associated with TCs generally has lower $\delta^{18}O$ than ordinary precipitation. Based on this mechanism, we established objective criteria to identify coral-based TC precipitation signals and reconstructed an index of TC precipitation for 1906–2012 CE. We then evaluated associations between this index and major climate drivers, including the AMO, solar variability, ENSO, and the PDO. These results provide new constraints on the decadal variability of TC activity and modulation by large-scale climate factors.

2. Materials and Methods

2.1. Study Area and Coral $\delta^{18}O$ Record

The study site is situated within the transitional zone between the western margin of the Northwest Pacific and the northern South China Sea, a region profoundly influenced by TC activity from summer to autumn (Z. Q. Chen et al., 2025; W. N. Huang & Dong, 2019) (Figure 1a). China Meteorological Administration (CMA) observational data from 1906 to 2012 indicate that approximately 27.4% of TC tracks passed within a 500 km radius of the study area. Adjacent to the Luzon Strait—a primary conduit for Pacific TCs entering the South China Sea between June and November—the site is ideally positioned to capture oceanic and precipitation signals associated with land-falling TCs along the southern Chinese coast (J. R. Sun et al., 2019). TC occurrence is also concentrated from June

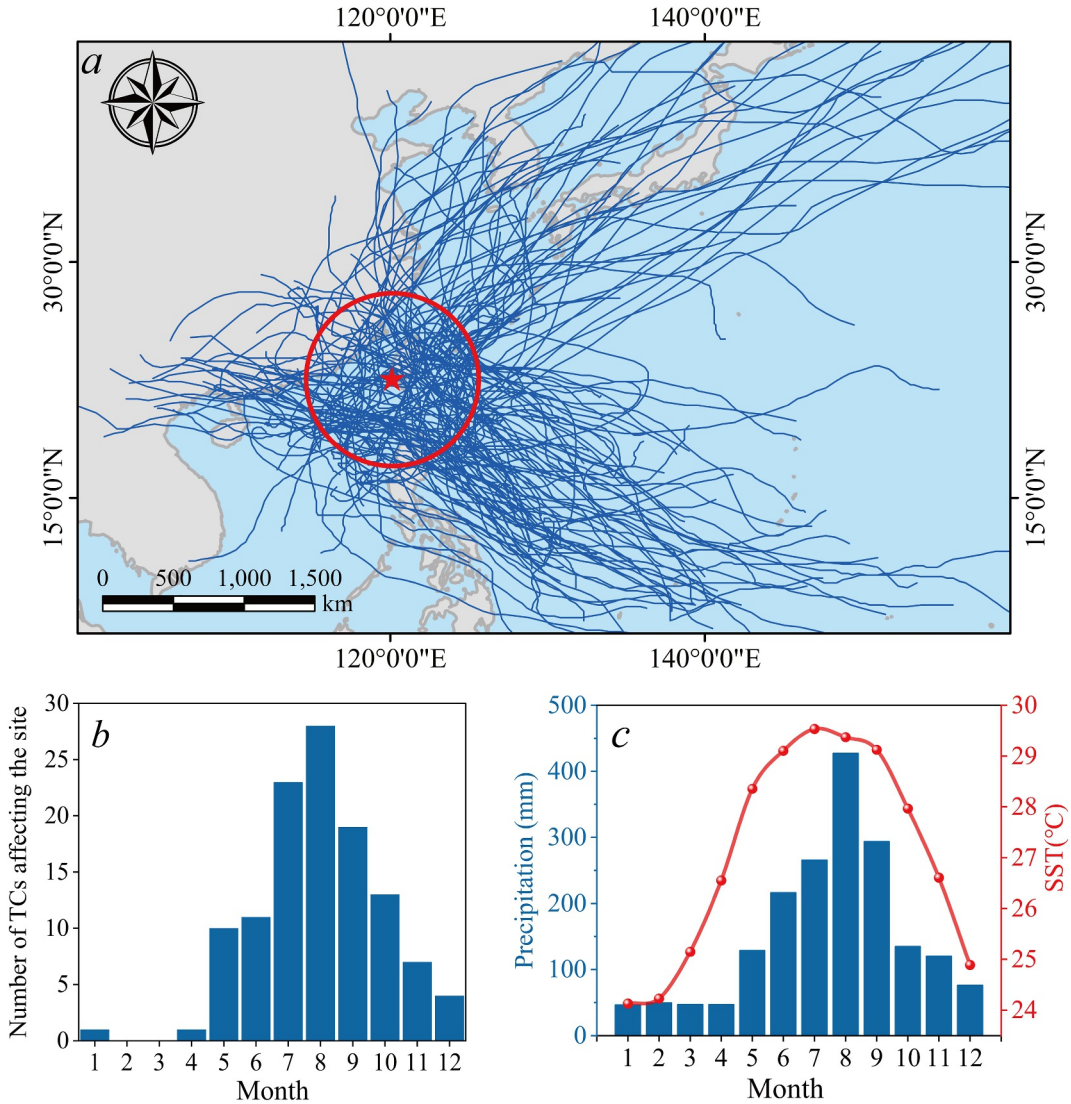


Figure 1. Seasonal and spatial characteristics of TCs affecting the coral sampling site. (a) Study area and the sampling location of the *Porites* coral core (red star), showing the tracks of TCs that affected the site during 1998–2012 CE. Distances between TCs and the sampling site are calculated using the Haversine formula. All TCs entered the 500 km radius of the sampling site at some point during their lifetimes. The red circle indicates the 500 km radius used to identify TCs influencing the site. (b) Monthly distribution of TCs affecting the coral site during 1998–2012 CE. Each TC is counted once based on the month of its closest approach to the site. (c) Climatological monthly sea surface temperature (red line) and precipitation (bars) at the Houbihu coral site.

to November (Figure 1b). Climatologically, the region exhibits a strongly seasonal precipitation regime. Instrumental records indicate that monthly mean precipitation remains relatively stable from January to April (approx. 46–49 mm). In contrast, precipitation during the TC season is highly concentrated, peaking in August with an average of ~427 mm, significantly exceeding totals in other months (Figure 1c). During the autumn transition, TC precipitation often interacts with the northeast monsoon and intraseasonal variability, leading to more episodic and spatially heterogeneous precipitation patterns (Zheng & Wang, 2023). This distinct hydroclimatic seasonality and direct exposure to TC pathways make the location particularly suitable for investigating TC precipitation signatures in the coral geochemical record.

This study utilizes a previously published, monthly resolved coral $\delta^{18}O$ record derived from a *Porites* specimen collected offshore from Houbihu (21.9°N, 120.7°E; Figure 1a). The $\delta^{18}O$ data were obtained from the publicly accessible NOAA World Data Service for Paleoclimatology. Comprehensive descriptions of the coral core

collection, sample preparation, and stable isotope measurement methodologies are detailed in the original published study associated with this data set (Ramos et al., 2020). The sampling site is distant from major riverine inputs, ensuring relatively stable background seawater salinity and minimizing confounding geochemical influences from terrestrial freshwater runoff on the coral archive. This coral geochemical data set was originally interpreted mainly in terms of SST, SSS, and precipitation variability (Ramos et al., 2020). Here, we use this data set to identify extreme hydrological anomalies associated with TC precipitation. Text S1 in Supporting Information S1 describes how the present analysis differs from the original study in research aim and methodological use of the coral $\delta^{18}O$ record.

2.2. Instrumental Data and Climate Indices

To assess environmental influences on the coral $\delta^{18}O$ record, monthly SST data were sourced from the HadISST data set (1° × 1° resolution; 1870–present) to correct for the temperature effect on coral $\delta^{18}O$. Monthly SSS data for evaluating regional hydrological variability were obtained from the UK Met Office EN4 (UKMO EN4) data set (1° × 1° resolution). Local monthly SST and SSS values for 1998–2012 were extracted from the KNMI Climate Explorer platform (https://climexp.knmi.nl; accessed 11 March 2025). Daily precipitation data (1998–2012 CE), which provide the mechanistic link between TC precipitation and the coral proxy, were obtained from the Hengchun County Meteorological Bureau (22.0°N, 120.7°E).

TC events affecting the study site were identified and validated using multiple observational sources. TC track and timing data were acquired from the CMA Tropical Cyclone Data Center. The distance between each TC center and the coral site was calculated using the Haversine formula to select TCs within a defined impact radius during 1998–2012 (Ying et al., 2014). An independent validation of TC activity was performed using the historical TC warning records issued by the Central Weather Administration (CWA) of Taiwan (1958–2012 CE) (https://rdc28.cwa.gov.tw).

To analyze the climatic drivers of TC precipitation variability, several key indices were employed. Monthly ENSO, PDO, and AMO time series were derived from HadISST data to ensure internal consistency. Monthly mean 200 hPa zonal wind (100°E−180°E, 0°N–25°N) and 500 hPa geopotential height (120°E−150°E, 10°N–40°N) from NOAA Twentieth Century Reanalysis V3 (20CR V3) were analyzed as proxies for Walker-circulation-related upper-level zonal flow and the intensity of the western North Pacific subtropical high (WNPSH), respectively. These data sets were obtained through the KNMI Climate Explorer (https://climexp.knmi.nl; accessed 14 August 2025). Solar activity was represented by the annual sunspot number series (1906–2012 CE) released by the Solar Influences Data Analysis Center (SIDC) at the Royal Observatory of Belgium (Clette & Lefèvre, 2015).

2.3. Derivation of Coral $\Delta\delta^{18}O$ and Gradient Metrics

The coral $\delta^{18}O$ is a function of both SST and the oxygen isotope composition of seawater ($\delta^{18}Osw$) (Thompson et al., 2022; Walter et al., 2023). To isolate the hydrological component, the seawater $\delta^{18}O$ anomaly ($\Delta\delta^{18}O$) was calculated. This parameter is derived by removing the temperature-dependent fractionation from the measured coral $\delta^{18}O$, based on the established paleotemperature equation for *Porites* corals rearranged as follows (Grossman & Ku, 1986):

$$\Delta\delta^{18}O = \delta^{18}O - (a \times SST + b)$$

Where a and b are the empirically determined slope and intercept of the local $\delta^{18}O$–SST calibration, respectively.

In tropical marine settings, $\Delta\delta^{18}O$ primarily reflects freshwater input. While common convective precipitation can lower seawater $\delta^{18}Osw$, the intense precipitation associated with TCs produces a more pronounced negative $\Delta\delta^{18}O$ anomaly (Sánchez-Murillo et al., 2019; C. J. Sun et al., 2022). To optimally capture these signals, both the absolute $\Delta\delta^{18}O$ value and its monthly rate of change (temporal gradient) were utilized as complementary indicators (Han et al., 2024). The cumulative $\Delta\delta^{18}O$ record integrates the net freshening effect over time, whereas its gradient is particularly sensitive to abrupt, short-lived excursions driven by individual, high-intensity TC precipitation events (Kilbourne et al., 2011; C. J. Sun et al., 2022; Thoppil, 2025). This dual-parameter approach enhances the detection and attribution of TC-related hydrographic anomalies within the coral record.

2.4. Identification of TC Precipitation

TC precipitation was quantified as the cumulative precipitation recorded during periods when a TC influenced the study site. Based on TC best-track data from the CMA, events whose centers passed within a 500 km radius of the coral site were identified. Daily precipitation occurring within the corresponding impact window for each identified TC was aggregated to calculate the event-total TC precipitation. This 500 km operational threshold was chosen to encompass the broad spatial extent of precipitation fields associated with TCs, which often extend significantly beyond the cyclone's core (Kumar et al., 2025; Qin et al., 2024). To ensure robustness and consistency, TC records from the CWA of Taiwan were used as an independent reference data set for validation. For the final analysis, only TC events that were consistently identified in both the CMA and CWA records and that produced a total precipitation exceeding 150 mm were retained. This combined criterion enhances the reliability of the event catalog used for calibrating and validating the coral proxy.

2.5. Detection Method

Han et al. (2024) developed a coral-based method for identifying and reconstructing a TC index using $\Delta\delta^{18}O$ and the gradient of $\Delta\delta^{18}O$. Following this framework, we applied modifications for the Houbihu record: TC identification was restricted to the regional TC season, spanning June to November. Correspondingly, in each year, the coral $\Delta\delta^{18}O$ and the gradient of $\Delta\delta^{18}O$ used were also limited to the same June–November interval. The rationale for selecting this seasonal window is provided in Text S3 and Figure S2 in Supporting Information S1.

Specifically, when either monthly $\Delta\delta^{18}O$ or the gradient of $\Delta\delta^{18}O$ during the TC season fell below the corresponding mean—1 SD threshold, the coral proxy anomaly was counted as one coral-based TC signal. If both indicators crossed their thresholds within the same month, only one signal was counted. The TC index was calculated by summing the number of below-threshold occurrences within each year. The interannual calibration skill of the threshold method using two indicators was evaluated by correlating the annual TC index derived from the coral record with the corresponding instrumental TC series.

3. Results and Discussion

3.1. $\Delta\delta^{18}O$ as a Proxy for SSS and Precipitation: Implications for Hydrological Variability

The results of the $\delta^{18}O$–SST calibration are provided in Text S2 in Supporting Information S1. To evaluate the applicability of the $\Delta\delta^{18}O$ proxy in this study, we compared the Houbihu coral $\Delta\delta^{18}O$ record with local instrumental SSS and precipitation during 1998–2012 CE. The relevant time series were smoothed using a 1 year running mean to reduce seasonal variability and short-period local fluctuations. The smoothed coral $\Delta\delta^{18}O$ record is significantly positively correlated with SSS ($r = 0.58$, $p < 0.0001$; Figure 2b), indicating that this record captures low-frequency changes in SSS (Pfeiffer et al., 2019; Thompson et al., 2022; Todorović et al., 2024). Instrumental precipitation and SSS show a significant negative correlation at the same smoothed timescale ($r = -0.56$, $p < 0.0001$; Figure 2c), consistent with surface freshening during wetter intervals. The smoothed coral $\Delta\delta^{18}O$ record is also significantly negatively correlated with precipitation ($r = -0.57$, $p < 0.0001$; Figure 2d). As a hydrological indicator of the surface freshwater balance, SSS can also integrate the effects of ocean advection, mixing, and entrainment (Hochet et al., 2025; Laurindo et al., 2024). This complexity does not obscure the significant correspondence between the Houbihu coral $\Delta\delta^{18}O$ record and instrumental hydroclimatic variability at the smoothed timescale, supporting the reliability of this proxy in the study area.

3.2. Modern Coral Record

Previous studies have demonstrated that coral-based TC reconstructions are subject to two categories of mismatch: omission errors, in which TCs meeting the instrumental screening criterion are not captured by the coral proxy; and false positives, in which the coral proxy falls below the defined threshold without a corresponding TC (Kilbourne et al., 2011). Furthermore, studies have shown that precipitation maxima, SSS variations, and negative coral $\Delta\delta^{18}O$ anomalies may exhibit offsets of 0–2 months at monthly resolution (Chen, Deng, et al., 2023, Chen, Guo et al., 2023; Deng et al., 2009, 2014; Garas et al., 2023). This uncertainty arises primarily from precipitation input variability, freshwater dilution and mixing processes, coral skeletal recording processes, and monthly age-model and sampling-averaging uncertainties, and cannot be eliminated in monthly resolved

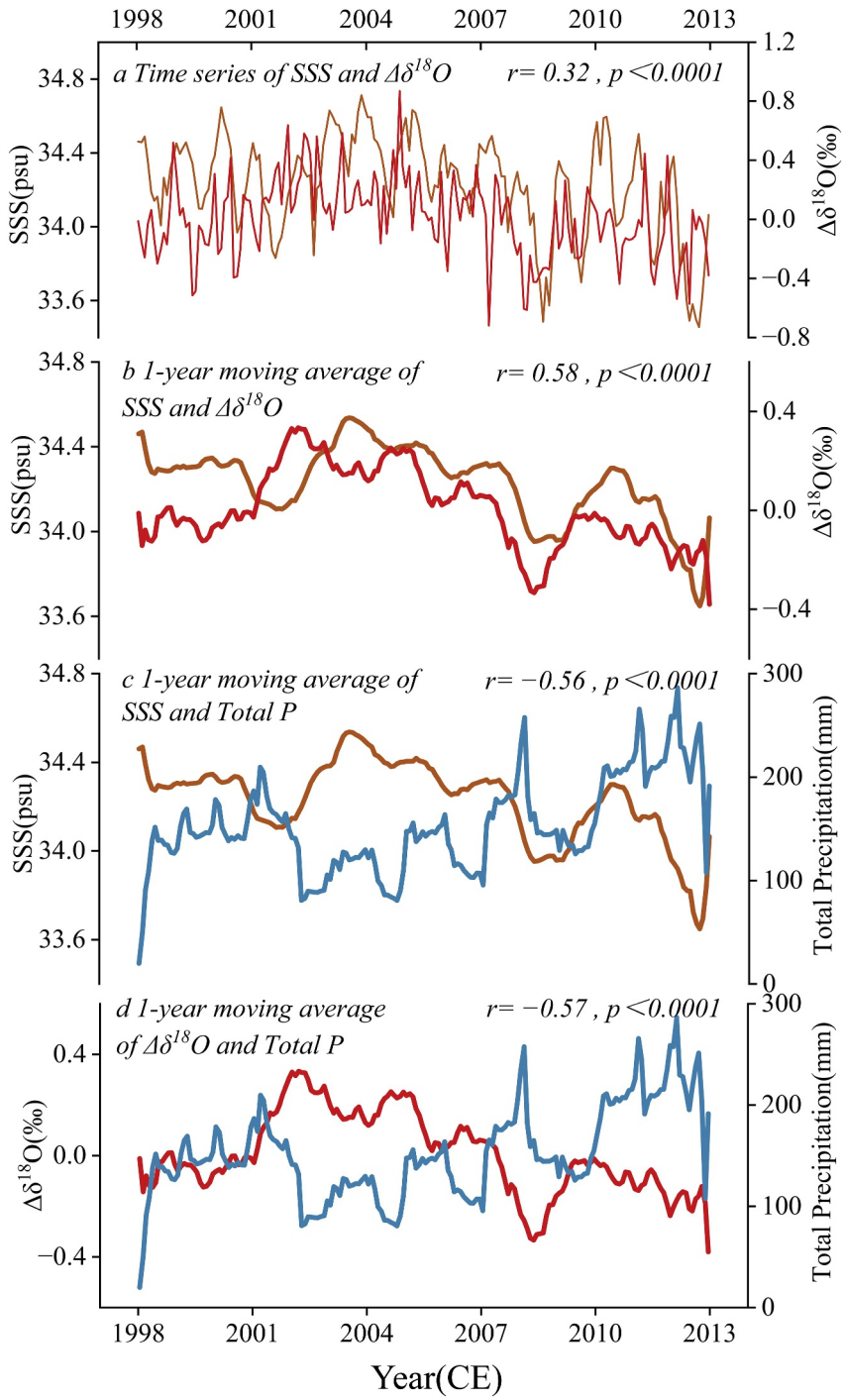


Figure 2. Time-series variations in sea surface salinity (SSS), precipitation, and *Porites* coral $\Delta\delta^{18}O$ in Houbihu during 1998–2012 CE. (a) Raw monthly SSS and coral $\Delta\delta^{18}O$. (b) One year running means of SSS and coral $\Delta\delta^{18}O$. (c) One year running means of SSS and precipitation. (d) One year running means of coral $\Delta\delta^{18}O$ and precipitation. Correlations among these variables are annotated in the panels. Brown, blue, and red lines represent SSS, precipitation, and coral $\Delta\delta^{18}O$, respectively.

coral record (Cahyarini et al., 2008; Lawman et al., 2020; Todorović et al., 2024; Walter et al., 2023). Accordingly, the blue bars in Figure 3 are assigned a temporal window of 0–2 months to account for this monthly-scale phase uncertainty.

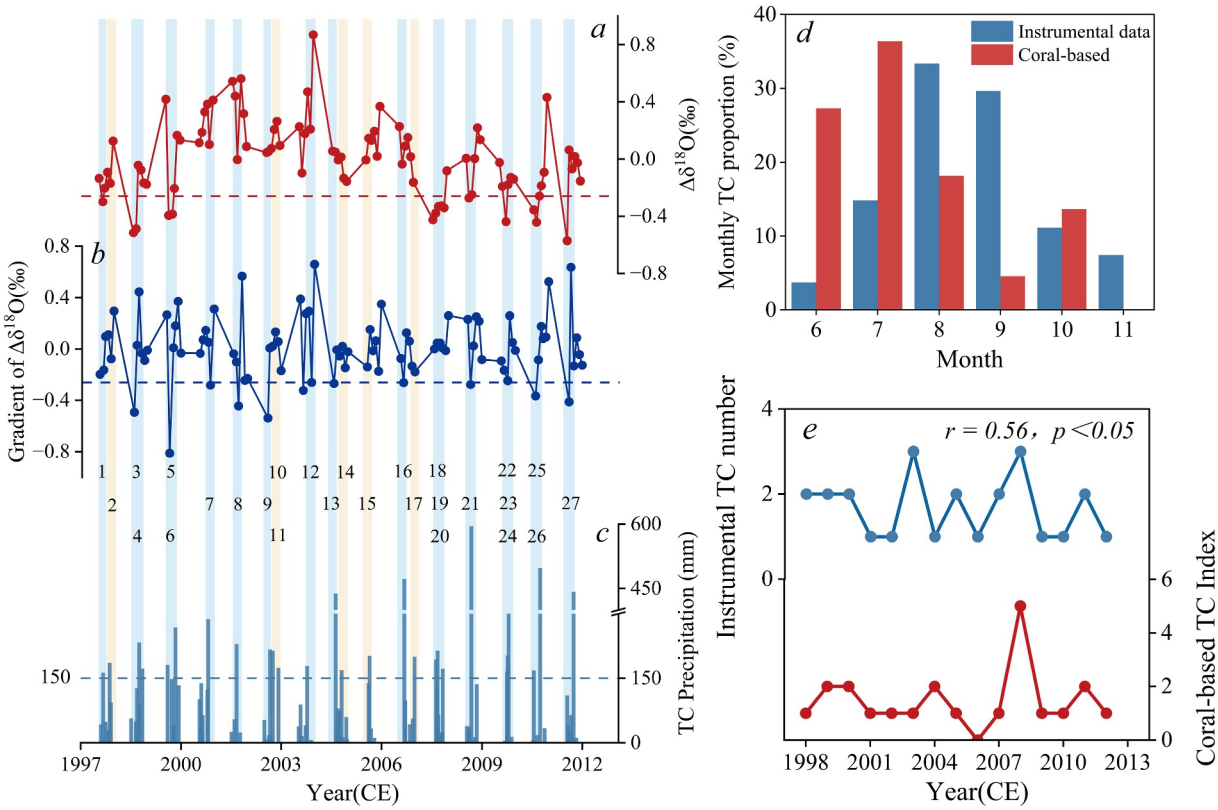


Figure 3. Comparison of Houbihu coral geochemical record with TC precipitation records during June–November of 1998–2012 CE. (a) $\Delta\delta^{18}O$. (b) The gradient of $\Delta\delta^{18}O$. (c) Precipitation associated with individual TCs. Numbers in panel (c) correspond to the TCs listed below the figure. (d) Monthly proportions of TCs recorded by the instrumental and coral record. Red and blue dashed lines represent the mean—1 SD thresholds for $\Delta\delta^{18}O$ and the gradient of $\Delta\delta^{18}O$, respectively. (e) Annual comparison of TC activity between the coral and instrumental records. Light blue and light yellow shading indicate TCs identified and not identified by the coral-based criteria, respectively.

Before applying the 150 mm criterion, we evaluated the sensitivity of the modern calibration to the choice of TC precipitation threshold. Threshold-sensitivity tests showed that the 150 mm TC precipitation threshold yielded the strongest and only statistically significant correlation between the coral-based and instrumental TC series ($r = 0.56$, $p < 0.05$; Table S1 in Supporting Information S1). Following the methodology outlined in Section 2.5, 27 instrumental TCs during 1998–2012 CE exceeded the 150 mm precipitation threshold (Figure 3). A total of 24 coral anomalies—defined as instances where $\Delta\delta^{18}O$ or its gradient fell below the mean—1 SD threshold—were identified. Among these, 21 anomalies corresponded to instrumental TCs, yielding a detection rate of 77.8% (blue bars in Figure 3); the remaining six instrumental TCs were not captured by either coral indicator (yellow bars in Figure 3). Within the TC season, three below-threshold coral anomalies lacked a corresponding instrumental TC with precipitation exceeding 150 mm, resulting in a false-positive rate of 12.5% (3/24) (2004 and 2008 CE). The most pronounced mismatch occurred in 2008, when three TCs satisfied the precipitation criterion yet coral $\Delta\delta^{18}O$ remained persistently depressed below the threshold for five consecutive months, suggesting that prolonged freshwater influence or overlapping TC signals may have obscured a clean one-to-one correspondence between individual anomalies and discrete TCs in that year (TCs 18, 19, and 20 in Figure 3). Notably, $\Delta\delta^{18}O$ and the

gradient of $\Delta\delta^{18}O$ exhibit clear complementarity in TC detection. During 2001–2006 CE, $\Delta\delta^{18}O$ itself showed no below-threshold anomalies. This was likely related to the persistently positive Niño3.4 background during this interval (Figure 2c in Supporting Information S1). In contrast, the gradient of $\Delta\delta^{18}O$ fell below the threshold on several occasions during the same interval and corresponded to multiple instrumental TCs, demonstrating that the gradient indicator retains sensitivity to TC signals even when the absolute $\Delta\delta^{18}O$ value is elevated or when negative anomalies are insufficiently pronounced to exceed the threshold on their own (Figure 3b). Overall, the majority of TCs produced detectable hydrological imprints in coral $\Delta\delta^{18}O$ or the gradient of $\Delta\delta^{18}O$, consistent with findings from previous studies (Han et al., 2024, 2026).

The monthly resolved coral record is inherently subject to calendar-month assignment uncertainties, resulting in apparent timing offsets of approximately 0–2 months in event matching. Our results are consistent with this characteristic: coral anomalies and instrumental TC occurrences show imperfect alignment in their monthly distributions (Figure 3d), with the coral-based TC signals tending to occur slightly earlier. In a timing-sensitivity test, shifting the coral-based TC signals forward by 1 month later substantially improved the agreement between their monthly distribution and that of the instrumental TCs ($r = 0.85$, $p < 0.05$; Figure S3 in Supporting Information S1). Nevertheless, uncertainties in monthly timing and phase remain. Another limitation of the monthly resolved coral record is that it cannot distinguish multiple TC precipitation events occurring within the same month; the only such case during the modern calibration interval occurred in September 2010, when three instrumental TCs exceeded the 150 mm precipitation threshold but were recorded as a single combined hydrological anomaly (TCs 22, 23, and 24 in Figure 3). These phase and resolution uncertainties render monthly coral indicators unsuitable for strict month-by-month reconstruction of individual TCs. However, annual aggregation reduces the influence of phase uncertainty on event detection (Pfeiffer et al., 2019). During 1998–2012 CE, TC counts derived independently from the coral indicators and instrumental records are significantly correlated at the annual scale ($r = 0.56$, $p < 0.05$; Figure 3e), confirming that this approach yields more stable and reliable calibration skill at annual resolution (Han et al., 2026).

Considering that the June–November TC season substantially overlaps with the regional wet season, contributions from non-TC precipitation to some coral $\Delta\delta^{18}O$ anomalies cannot be entirely excluded (Shen et al., 2005). However, previous isotope and coral studies have shown that TC precipitation is typically more depleted in $\delta^{18}O$ and is therefore more likely to generate pronounced negative anomalies in coral $\delta^{18}O$ (Han et al., 2024, 2026; Jackisch et al., 2022; Kilbourne et al., 2011). Modern observations further show that, after controlling for non-TC precipitation, TC precipitation remains strongly and negatively correlated with coral $\Delta\delta^{18}O$ (*partial* $r = -0.48$, $p = 0.07$; Figure S4d and Text S4 in Supporting Information S1), whereas the annual non-TC precipitation index is essentially uncorrelated with the coral-based TC index ($r = -0.03$, $p = 0.91$; Figure S4f and Text S4 in Supporting Information S1). These results indicate that, although the limited length of the modern calibration interval and the monthly resolution constrain complete separation of different precipitation sources, non-TC wet-season precipitation is insufficient to explain the interannual variability of the coral-based TC index, supporting its interpretation as primarily reflecting TC-related hydrological signals.

3.3. Decadal-Scale Reconstruction and Low-Frequency Climate Controls

Based on the response of anomalously low values in coral $\Delta\delta^{18}O$ and the gradient of $\Delta\delta^{18}O$ to TC precipitation during the modern calibration period, we used a threshold approach with two indicators to reconstruct a coral-based index of TC precipitation variability in the study region for 1906–2012 CE. For each year, anomalies in either $\Delta\delta^{18}O$ or the gradient of $\Delta\delta^{18}O$ that fell below their corresponding mean—1 SD thresholds during June–November were identified as TC precipitation signals recorded in the coral record. If both indicators crossed the threshold in the same month, they were counted as a single signal, and the number of these signals was used as the TC index for that year (Figures 4a–4c).

3.3.1. Decadal-Scale Variability of TC Activity

To evaluate the low-frequency variability of the TC index, we compared it with the TC anomalous count affecting Taiwan compiled by Hung (2013) and the CWA record of TCs with event-total precipitation >150 mm at Hengchun Station during 1958–2012 CE (Figures 4d and 4e).

During 1906–2012 CE, the TC index shows pronounced decadal-scale variability (Figure 4c). The index was generally elevated during 1906–1949 CE, with a mean value of 2.70 years^{-1}. It reached high values in both the

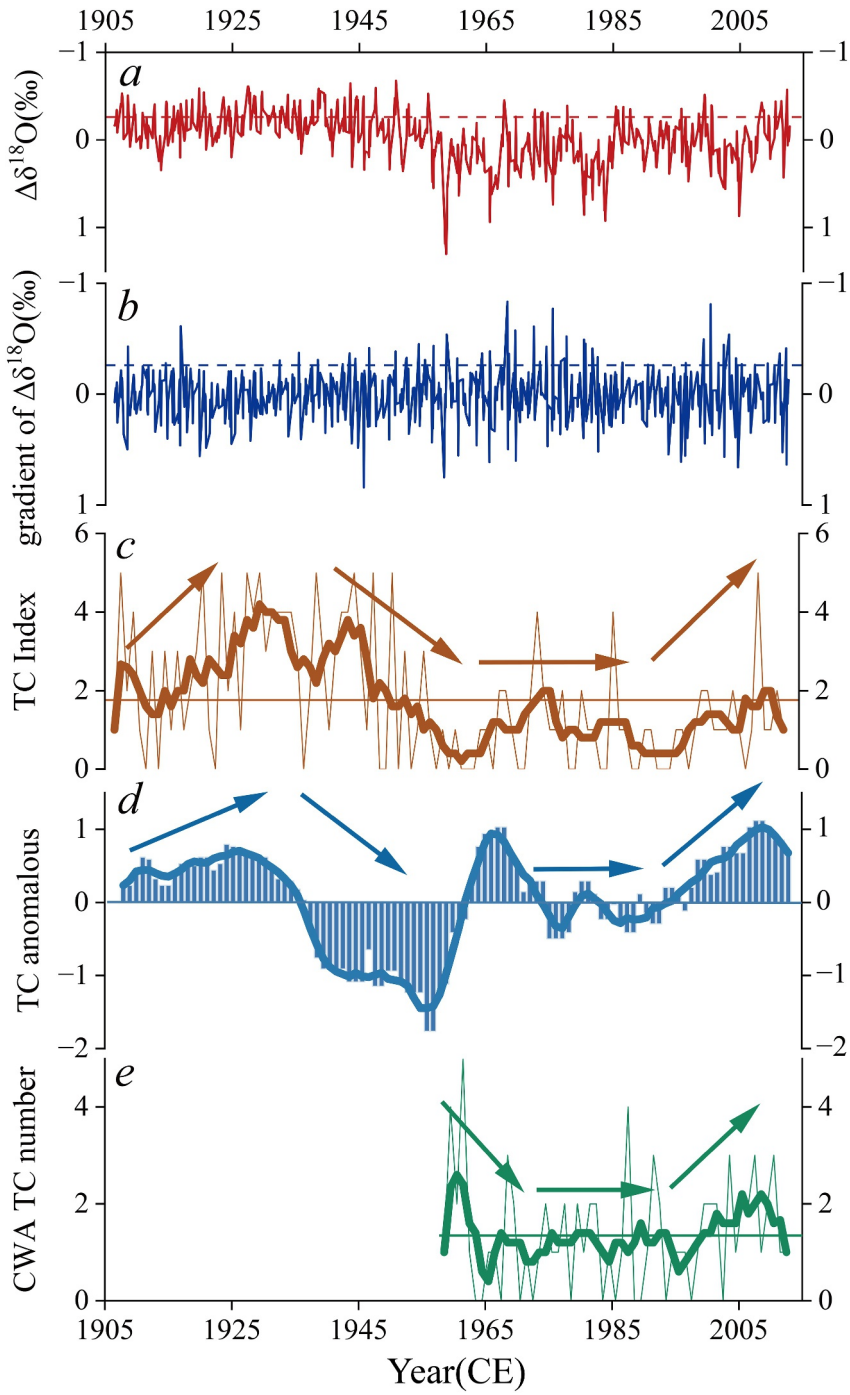


Figure 4. Coral-based reconstruction of the TC Index from 1906 to 2012 CE and comparison with Taiwan TC records. (a) $\Delta\delta^{18}O$; (b) the gradient of $\Delta\delta^{18}O$; (c) TC index; (d) TC anomalous count affecting Taiwan compiled by Hung (2013); (e) annual number of TCs with event-total precipitation >150 mm recorded at Hengchun Station by the Central Weather Administration during 1958–2012 CE. Horizontal solid lines indicate long-term means; dashed lines in (a) and (b) indicate the mean − 1 SD thresholds. Thick lines in (c), (d), and (e) indicate 5-year running means.

1920s and 1930s, with decadal means of 3.20 years^{-1}, and remained relatively high in the 1940s, with a mean value of 2.60 years^{-1}. After 1950, the TC index decreased markedly on decadal timescales. The mean value during the 1960s–1990s declined to 0.93 years^{-1}, with particularly low values in the 1960s and 1990s of 0.80 years^{-1} and 0.70 years^{-1}, respectively. Since the early 21st century, the TC index has partially recovered,

Table 1
Decadal Comparison of TC Frequency From Coral Reconstruction and Central Weather Administration Records

Decade	CWA TC Number (>150 mm)	TC frequency index (coral-based reconstruction)
1963–1972	0.8	0.9
1973–1982	1.4	1.4
1983–1992	1.3	0.8
1993–2002	1	0.9
2003–2012	1.9	1.5

increasing to 1.46 years^{-1} during 2000–2012 CE, although this remains lower than the high index interval of 1906–1949 CE. Overall, the record indicates three major phases in TC precipitation activity in the study region: elevated activity in the early 20th century, reduced activity during the mid-to-late 20th century, and partial recovery in the early 21st century. Sensitivity tests further support the stability of this low-frequency pattern (Figure S5 and Text S5 in Supporting Information S1).

This low-frequency pattern is partly supported by independent Taiwan TC records (Figures 4d and 4e). The TC anomalous count was generally positive during 1906–1929 CE, with a mean value of 0.52, including a 1920s mean of 0.62, supporting relatively active TC conditions around Taiwan during the early 20th century (Figure 4d). For the instrumental period, the CWA record shows that the mean number of TCs was 1.10 events yr^{-1} during 1970–1999 CE and increased to 1.77 events yr^{-1} during 2000–2012 CE (Figure 4e). Correspondingly, TC index increased from 0.97 years^{-1} during 1970–1999 CE to 1.46 years^{-1} during 2000–2012 CE, indicating that both records capture an enhancement of TC precipitation activity in the early 21st century.

Some differences among the records remain. For example, the TC anomalous count became negative in the 1930s (Figure 4d), whereas TC index remained high during this interval (Figure 4c). For the instrumental period, the 1983–1992 CE interval represents the main exception in the 10-year mean comparison between the TC index and the CWA record (Table 1), indicating that the two records are not fully synchronous across all decades. Overall, these discrepancies do not obscure the major low-frequency pattern captured by the TC index.

3.3.2. Spectral Characteristics of Reconstructed TC Activity

The variability of TC activity is unlikely to be explained solely by the random occurrence of individual TCs or local precipitation variability; instead, it likely reflects decadal-to-multidecadal modulation of regional TC activity by large-scale ocean–atmosphere variability and external forcing. Spectral analysis of the reconstructed series reveals enhanced power at periodicities of ∼2–6, ∼11, ∼36, and ∼64 years (Figure S6 in Supporting Information S1). These features suggest that the reconstruction contains substantial low-frequency variability in addition to interannual fluctuations.

3.3.3. Decadal Covariability With Solar Activity

Spectral analysis of the reconstructed series reveals enhanced power at a periodicity of ∼11 years. Sunspot number anomalies were used as a proxy for solar activity and compared with the reconstructed TC activity. Results indicate a significant negative correlation at the decadal scale ($r = -0.41$, $p < 0.001$; Figure 5a) over 1906–2012, whereas the interannual correlation is markedly weaker ($r = -0.26$, $p < 0.001$). This contrast suggests stronger low-frequency covariation between solar activity and TC activity at the decadal scale. This aligns with the "low solar activity–high TC activity" pattern reported in the literature and paleoclimate records from the Taiwan region, providing independent support for the decadal-scale relationship identified here (Hung, 2013).

To explore the circulation pathway underlying this low-frequency solar–TC relationship, we further examined the 200 hPa zonal wind, which serves as a proxy for Walker circulation related upper-level flow and is relevant to Northwest Pacific TC activity. A more detailed analysis shows that the correlation between solar activity and the 200 hPa zonal wind is weak at zero lag ($r = 0.19$, $p < 0.01$), indicating that the circulation response to solar forcing is not synchronous. In contrast, lag-correlation analysis shows that when solar activity leads by 3–5 years, its relationship with both the 200 hPa zonal wind and TC index becomes substantially stronger, with correlation

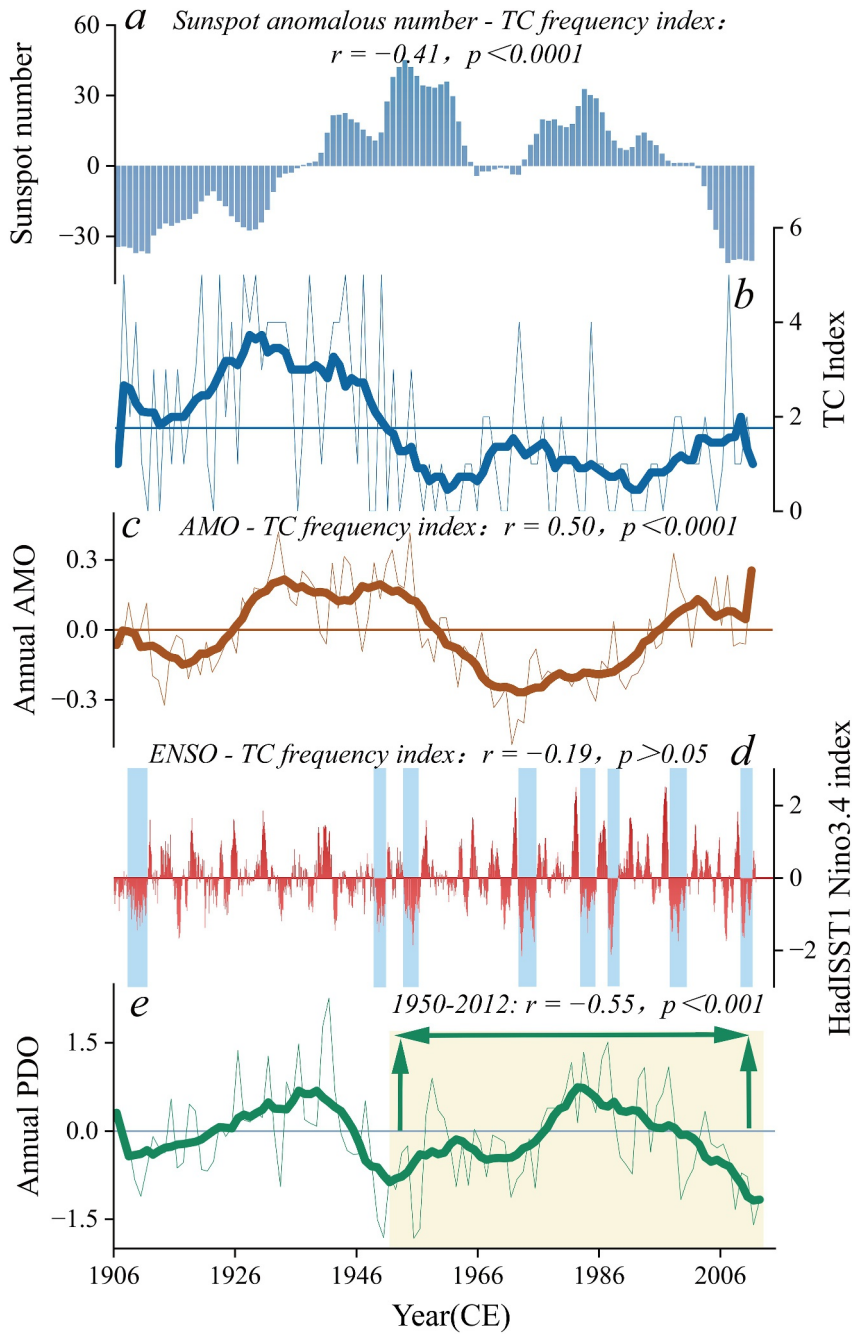


Figure 5. Coral-based reconstruction of TC Index (1906–2012 CE) and its relationship with climate indices. (a) Sunspot number anomaly (11-year running mean). (b) TC index (thin line), with the 11-year running mean (thick line) and the long-term mean (horizontal line). (c) Annual-mean Atlantic Multidecadal Oscillation index, with the 11-year running mean (thick line). (d) Niño3.4 index; blue shading indicates La Niña conditions (Niño3.4 < 0). (e) Annual-mean Pacific Decadal Oscillation (PDO) index, with the 11-year running mean (thick line). Pale yellow shading indicates a strong negative correlation between the PDO and TC since 1950.

coefficients of 0.35–0.44 for solar activity versus zonal wind and −0.66 to −0.74 for solar activity versus TC index (Figure 6b). This suggests that solar activity is more likely to influence TC activity through delayed modulation of the tropical Pacific background state and related circulation processes, rather than through direct contemporaneous forcing (Elsner & Jagger, 2008; Huo et al., 2021; Meehl et al., 2009; Misios et al., 2019). This interpretation is consistent with previous studies showing that approximately 11-year solar variability can induce

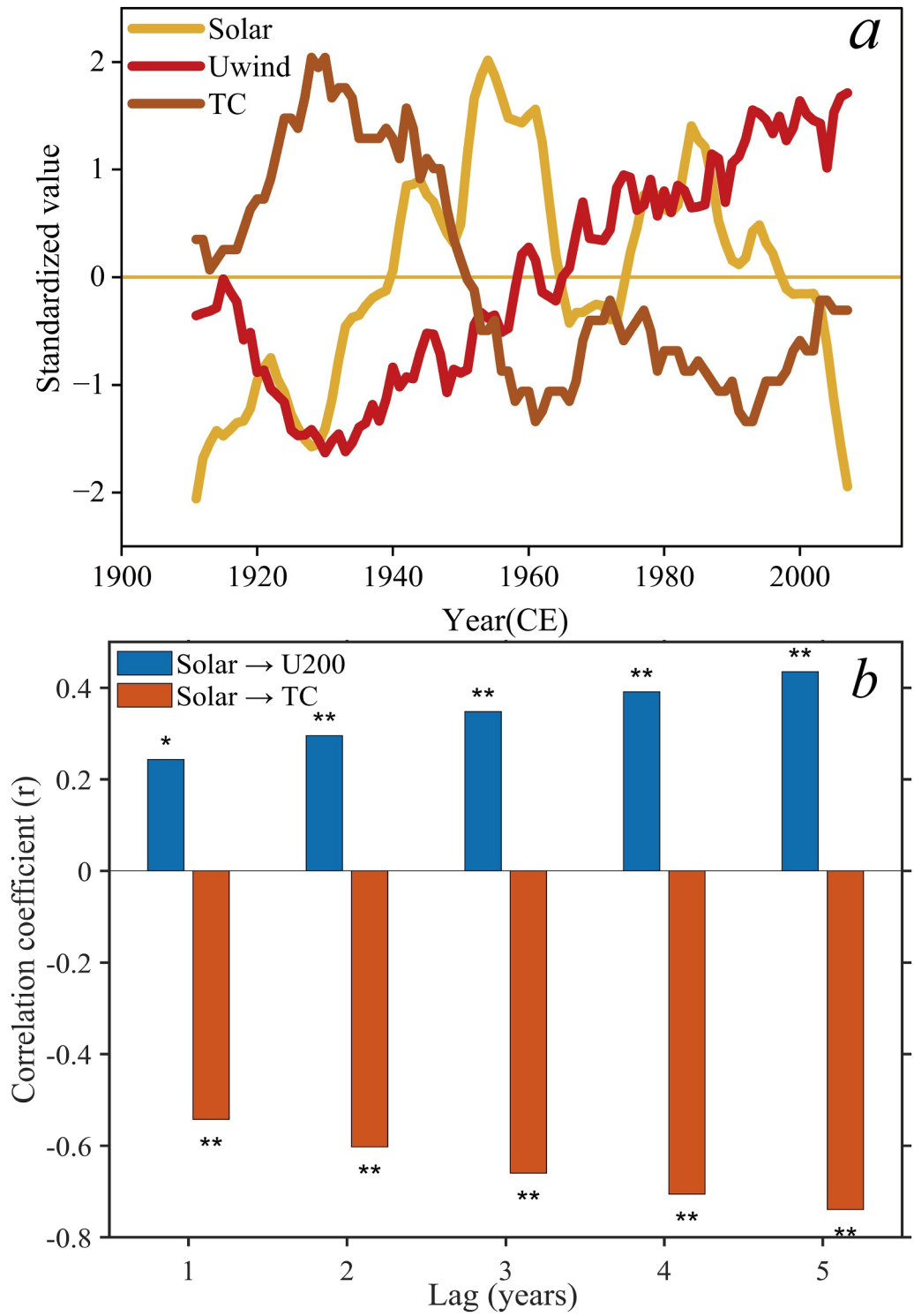


Figure 6. Relationships among solar activity, Walker circulation, and reconstructed TC Index. (a) Standardized time series of the 11-year running mean solar activity, annual 200 hPa zonal wind (used here as a proxy for the Walker circulation), and reconstructed TC index. (b) Lagged correlations between solar activity and 200 hPa zonal wind, and between solar activity and TC activity, for lags of 1–5 years. Positive lags indicate that solar activity leads 200 hPa zonal wind and TC index. Asterisks denote statistical significance ($p < 0.05$, $p < 0.01$).

delayed air–sea responses in the tropical Pacific and modulate the Walker circulation on decadal timescales (D. L. Li et al., 2023; S. Li, Li, & Ling, 2023). In summary, our results support a mechanism in which solar activity affects the TC activity in the Northwest Pacific primarily through low-frequency, delayed ocean–atmosphere coupling, rather than by directly controlling individual TCs.

3.3.4. Multidecadal Covariability With AMO

Spectral analysis reveals enhanced power at periodicities of ∼64 years, consistent with the characteristic multidecadal variability range of the AMO. To further evaluate this correspondence, we compared the annual-mean AMO index with the coral-based reconstruction of TC activity. The results show a significant positive correlation ($r = 0.50$, $p < 0.001$; Figure 5c) over 1906–2012 CE, indicating significant decadal-to-multidecadal covariability between the two records.

Previous studies have shown that the AMO can influence large-scale circulation in the tropical Pacific through an atmospheric bridge mechanism (An et al., 2021; McGregor et al., 2014; J. W. Zhao et al., 2024). Specifically, SSTA in the North Atlantic can modulate the tropical energy balance and convective distribution, thereby affecting the Walker circulation and its associated wind field structure (Jiang & Li, 2021; C. Sun et al., 2020). Such inter-basin interactions can further alter moisture transport and convergence over the western Pacific, influencing the environmental conditions associated with TC precipitation (J. W. Zhao et al., 2024). Based on this metric, the results show a significant negative correlation between the AMO and zonal wind ($r = -0.50$, $p < 0.001$; Figure 7b), indicating that AMO variability is closely linked to changes in Walker circulation strength. In addition, the zonal wind exhibits a strong negative correlation with the TC index ($r = -0.82$, $p < 0.001$; Figure 7c), suggesting that variations in Walker circulation play a key role in modulating TC precipitation. It should be noted that the reconstruction spans only ∼1 century, which likely captures no more than a single phase of multidecadal variability. The modulatory influence of the AMO should be evaluated using longer records and replication across multiple sites.

3.3.5. Non-Stationarity in the Impacts of ENSO and PDO on TC Activity

Spectral analysis reveals significant power peaks in TC index at the 2–6-year and ∼36-year timescales, corresponding to the interannual variability of ENSO and the decadal variability of the PDO, respectively. However, the influences of ENSO and the PDO on TC activity exhibit pronounced non-stationarity over the study period. The annual mean Niño3.4 index shows only a modest and statistically non-significant inverse relationship with TC activity ($r = -0.19$, $p = 0.055$; Figure 5d), suggesting that this overall linear relationship may obscure distinct phase-dependent modulation across different periods. Specifically, during 1906–1949, the PDO is significantly positively correlated with TC activity ($r = 0.63$, $p < 0.001$; Figure 5e), whereas this relationship reverses after 1950. During 1950–2012, the PDO becomes significantly negatively correlated with TC activity ($r = -0.55$, $p < 0.001$; Figure 5e). This non-stationary relationship may be associated with interdecadal changes in the background climate state and the evolution of ENSO characteristics.

Previous studies have demonstrated that the teleconnection effects of climate drivers are strongly background-state dependent (Li, Xiao, & Zhao, 2023; Sena et al., 2025; L. Shi et al., 2024; C. Zhou et al., 2024). Our results indicate that during 1906–1949, the large-scale circulation was relatively weak, characterized by weak upper-level zonal flow (with 200 hPa mean zonal wind speeds of only ∼0.22 m/s) and a very low occurrence frequency of the WNPSH (∼6.8%) (Figures 8a and 8b). Under such a weak background state, PDO-related signals may be linked to TC activity through modulation of the WNPSH edge and associated regional circulation anomalies (C. Huang et al., 2022; Tian et al., 2023). In contrast, the Walker circulation strengthened significantly after 1950, with 200 hPa mean zonal wind speeds increasing to ∼1.04 m/s ($p < 0.0001$) (Figures 8a and 8b). Meanwhile, the WNPSH entered a phase of accelerated intensification, as indicated by an increase in the 500 hPa geopotential height trend from 0.18 m/yr to 0.28 m/yr ($p < 0.0001$), and a rise in the frequency of strong WNPSH occurrences from 6.8% to 41.3%. Furthermore, the post-1950 enhancement rate of the height field (0.28 m/yr) is substantially higher than that during the earlier period (0.18 m/yr) (Figures 8a and 8b). This pronounced strengthening and accelerated transition of the background circulation may have altered the efficiency of remote forcing and local atmospheric responses, thereby contributing to the observed reversal in the PDO–TC relationship (Scoccimarro et al., 2021; C. Wang et al., 2023).

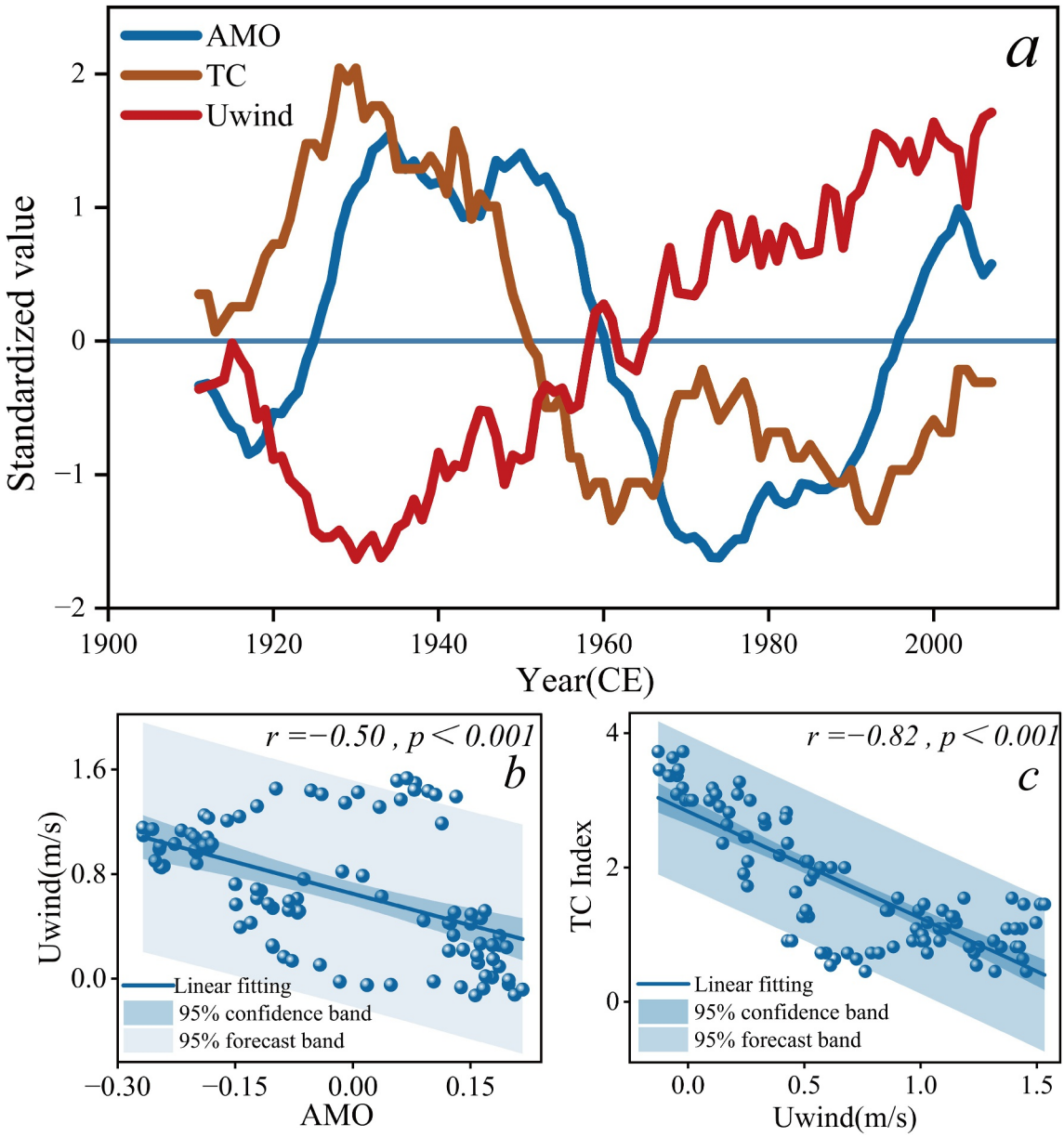


Figure 7. Atlantic Multidecadal Oscillation (AMO), Walker circulation, and reconstructed TC Index. (a) Standardized 11-year running mean time series of the AMO index, annual 200 hPa zonal wind, and reconstructed TC index during 1906–2012 CE. (b) Scatterplot of the 11-year running mean AMO index against 200 hPa zonal wind. (c) Scatterplot of the 11-year running mean 200 hPa zonal wind against reconstructed TC index, showing a significant negative correlation. Solid lines represent linear regressions, and shaded areas indicate the 95% confidence and prediction intervals.

Furthermore, the reversal in the influence of ENSO on TCs is likely associated with interdecadal changes in the dominant types of El Niño events (Figure 8c) (X. Chen, Deng, et al., 2023, Chen, Guo et al., 2023; J. Song et al., 2023; Tian et al., 2023). During 1906–1949, all seven identified El Niño events (Niño3.4 > 0.5°C) correspond to the central Pacific type, based on a simplified classification (Figure 8d) (Niño3.4 > Niño3). The associated mean TC index is 2.57 years^{-1}, which is close to the climatological mean for the same period (2.70 years^{-1}), suggesting a relatively weak suppression effect of CP-type events on TC activity (Figure 8e) (X. Chen, Deng, et al., 2023, Chen, Guo et al., 2023; Zhang et al., 2015). In contrast, El Niño events during 1950–2012 exhibit greater diversity, with the proportion of eastern Pacific (EP) type events (Niño3 > Niño3.4) increasing to 41.7% (Figure 8d). The mean TC index during EP-type events is only 0.60 years^{-1}, substantially lower than the climatological mean (1.11 years^{-1}) (Figure 8e). Consistent with previous studies, EP-type El Niño events tend to exert a stronger suppressing effect on

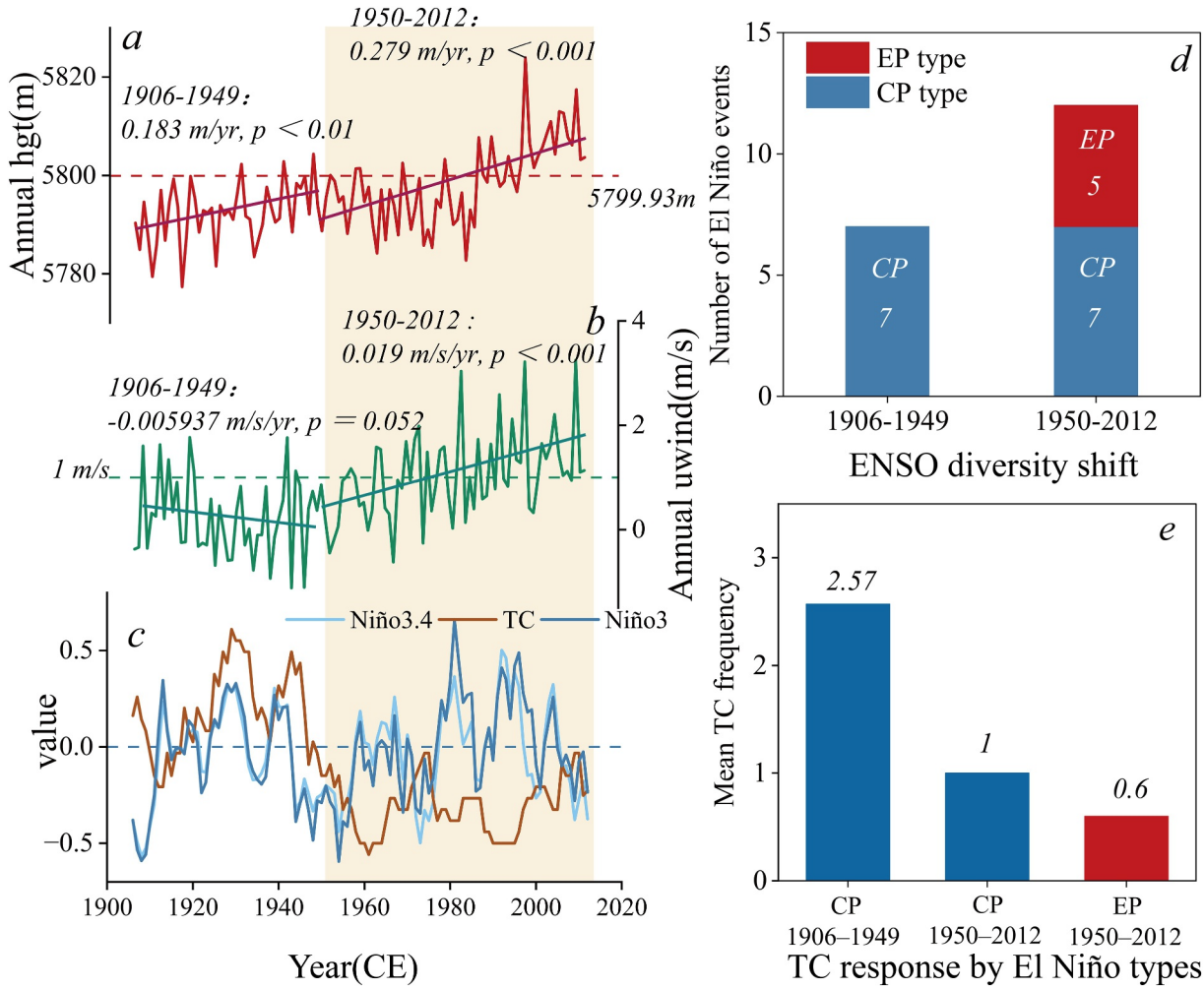


Figure 8. Interdecadal variations in the relationship between ENSO and reconstructed TC index, the evolution of ENSO event types, and associated large-scale background circulation influencing Pacific Decadal Oscillation and ENSO during 1906–2012. Pale yellow shading denotes the 1950–2012 CE interval, highlighting the period after the marked climatological transition around 1950. (a) Annual mean 500 hPa geopotential height over the western North Pacific (120°E−150°E, 10°N–40°N), representing the intensity of the western North Pacific subtropical high. Linear trends for the two periods and the climatological threshold (dashed line) are shown. (b) Annual mean 200 hPa zonal wind over the western Pacific (100°E−180°E, 0°N–25°N), representing the upper-level zonal circulation associated with the Walker circulation. Linear trends for the two periods and the reference threshold (1 m/s) are indicated. (c) Standardized time series of the 5-year moving averaged Niño3.4 index, Niño3 index and TC index. (d) Interdecadal changes in El Niño event types. Stacked bars show the number and proportion of central Pacific and eastern Pacific El Niño events in two periods (1906–1949 and 1950–2012 CE), based on a simplified classification criterion (Niño3.4 > Niño3 for CP; Niño3 > Niño3.4 for EP; Niño3.4 > 0.5°C). (e) Mean TC index associated with different types of El Niño events, illustrating distinct TC responses to different ENSO types.

TC activity by enhancing anomalous easterly winds and strengthening the WNPSH, whereas CP-type events have a relatively weaker influence on this circulation system (M. Chen et al., 2019; L. Wu et al., 2018; Yu et al., 2021). Therefore, these results indicate a clear interdecadal shift in the dominant type of El Niño events. CP-type events dominate in the early period, whereas both EP- and CP-type events occur in the later period, with an increasing proportion of EP events. Together with changes in the background circulation, this shift may provide a plausible explanation for the observed transformation in ENSO–TC modulation. More broadly, the climate–TC relationships identified above are also evident in two independent instrumental TC records from Taiwan, which show consistent associations with the AMO, solar activity, and PDO, as well as lower TC activity during EP-type than CP-type El Niño years (Text S6 and Figure S7 in Supporting Information S1).

4. Conclusions

This study identifies a modern-calibrated association between pronounced negative excursions in coral $\Delta\delta^{18}O$ from the Northwest Pacific and TC (precipitation exceeding 150 mm). Applying this method, we reconstructed

TC precipitation variability for 1906–2012 CE. The reconstruction reveals pronounced interdecadal variability, characterized by distinct phases: high activity in the early 20th century, a decline in the mid-century, and a partial recovery in recent decades. Multidecadal analysis indicates that this low-frequency variability significantly covaries with solar activity and the phase of the AMO. In contrast, ENSO and PDO generally show weaker correlations with annual-scale TCs, but their correlations have notably strengthened since the mid-20th century. This shift highlights their non-stationary influence on TC precipitation. This reconstruction offers a critical baseline for contextualizing recent trends and emphasizes the importance of low-frequency climate modes in modulating TC extreme precipitation.

Conflict of Interest

The authors declare no conflicts of interest relevant to this study.

Availability Statement

The original coral $\delta^{18}O$ data can be obtained from the NOAA NCDC World Data Center for Paleoclimatology at Ramos (2020). Sea surface temperature, SSS, ENSO, PDO, AMO, 200 hPa zonal wind, and 500 hPa geopotential height data for the study region were obtained through the KNMI Climate Explorer (https://climexp.knmi.nl). Daily precipitation data from Hengchun for 1998–2012 and historical TC warning records for Taiwan were obtained from the CWA of Taiwan (https://rdc28.cwa.gov.tw). TC track and timing information were obtained from the CMA Tropical Cyclone Data Center at Ying et al. (2014) (https://tcdata.typhoon.org.cn/zjljsjj.html). Annual sunspot numbers were obtained from the Solar Influences Data Analysis Center (SIDC) at the Royal Observatory of Belgium at Clette and Lefèvre (2015) (https://www.sidc.be/SILSO/datafiles). The data used and calculated in this study can be found at Shi and Jiang (2026).

Acknowledgments
This work was financially supported by the National Key R&D Program of China (Grant 2023YFF0804801), Guangxi Science and Technology Program (No. AD25069075), the National Natural Science Foundation of China (Grants 41976059 and 42265007), and the major talent project of Guangxi Zhuang Autonomous Region (GXR-1BGQ2424020). We thank Editor Prof. Nathalie Goodkin and two anonymous reviewers for their careful work and constructive suggestions, which greatly improved this manuscript.

References

Altman, J., Saurer, M., Dolezal, J., Maredova, N., Song, J. S., Ho, C. H., & Treydte, K. (2021). Large volcanic eruptions reduce landfalling tropical cyclone activity: Evidence from tree rings. *Science of The Total Environment*, *775*, 145899. https://doi.org/10.1016/j.scitotenv.2021.145899

An, X. H., Wu, B., Zhou, T. J., & Liu, B. (2021). Atlantic multidecadal oscillation drives interdecadal Pacific variability via tropical atmospheric bridge. *Journal of Climate*, *34*(13), 5543–5553. https://doi.org/10.1175/Jcli-D-20-0983.1

Bhatia, K., Baker, A., Yang, W., Vecchi, G., Knutson, T., Murakami, H., et al. (2022). A potential explanation for the global increase in tropical cyclone rapid intensification. *Nature Communications*, *13*(1), 6626. https://doi.org/10.1038/s41467-022-34321-6

Cahyarini, S. Y., Pfeiffer, M., Timm, O., Dullo, W.-C., & Schönberg, D. G. (2008). Reconstructing seawater $\delta^{18}O$ from paired coral $\delta^{18}O$ and Sr/Ca ratios: Methods, error analysis and problems, with examples from Tahiti (French Polynesia) and Timor (Indonesia). *Geochimica et Cosmochimica Acta*, *72*(12), 2841–2853. https://doi.org/10.1016/j.gca.2008.04.005

Cao, J., Feng, J., Zhao, H., Wang, B., Wu, L., & Wang, C. (2025). Comparable impacts of IPO and AMO on the decadal change of northern hemisphere tropical cyclone frequency. *Climate Dynamics*, *63*(1), 23. https://doi.org/10.1007/s00382-024-07523-5

Chen, F. J., Huang, C., Lao, Q. B., Zhang, S. W., Chen, C. Q., Zhou, X., et al. (2021). Typhoon control of precipitation dual isotopes in Southern China and its palaeoenvironmental implications. *Journal of Geophysical Research-Atmospheres*, *126*(14), e2020JD034336. https://doi.org/10.1029/2020JD034336

Chen, L., Wang, T., Sinha, A., Lin, F., Tang, H., Cheng, H., & Tan, L. (2024). A seasonally resolved stalagmite $\delta^{18}O$ record indicates the regional activity of tropical cyclones in Southeast China. *npj Climate and Atmospheric Science*, *7*(1), 168. https://doi.org/10.1038/s41612-024-00715-0

Chen, M., Yu, J. Y., Wang, X., & Jiang, W. (2019). The changing impact mechanisms of a diverse El Niño on the western Pacific subtropical high. *Geophysical Research Letters*, *46*(2), 953–962. https://doi.org/10.1029/2018GL081131

Chen, X., Deng, W., Xiao, H., Guo, H., Zeng, T., Zhao, J.-x., & Wei, G. (2023). Coral paleoclimate perspectives support the role of low-latitude forcing on the 4.2 ka BP event. *Geophysical Research Letters*, *50*(13), e2023GL104010. https://doi.org/10.1029/2023GL104010

Chen, X., Guo, Y.-P., Tan, Z.-M., & Zhao, J. (2023). Influence of different types of ENSO events on the tropical cyclone rainfall over the western North Pacific. *Climate Dynamics*, *60*(11), 3969–3982. https://doi.org/10.1007/s00382-022-06547-z

Chen, Z. Q., Chan, K. T. F., & Luo, Z. W. (2025). Statistical seasonal forecasting of tropical cyclone landfalls on Taiwan Island. *Atmospheric and Oceanic Science Letters*, *18*(2), 100554. https://doi.org/10.1016/j.aosl.2024.100554

Chu, P. S., Zhang, H. P., Chang, H. L., Chen, T. L., & Tofte, K. (2018). Trends in return levels of 24-hr precipitation extremes during the typhoon season in Taiwan. *International Journal of Climatology*, *38*(14), 5107–5124. https://doi.org/10.1002/joc.5715

Clette, F., & Lefèvre, L. (2015). SILSO *sunspot number V2.0* [Dataset]. *WDC-SILSO, Royal Observatory of Belgium*. https://doi.org/10.24414/qnza-ac80

Deng, W., Wei, G., Yu, K., & Zhao, J.-X. (2014). Variations in the timing of the rainy season in the northern South China Sea during the middle to late Holocene. *Paleoceanography*, *29*(2), 115–125. https://doi.org/10.1002/2012PA002417

Deng, W. F., Wei, G. J., Li, X. H., Yu, K. F., Zhao, J. X., Sun, W. D., & Liu, Y. (2009). Paleoprecipitation record from coral Sr/Ca and δ18O during the mid Holocene in the northern South China Sea. *The Holocene*, *19*(6), 811–821. https://doi.org/10.1177/0959683609337355

Donnelly, J. P. (2025). Reconstructing tropical cyclone activity from sedimentary archives. *Annual Review of Earth and Planetary Sciences*, *53*(1), 251–281. https://doi.org/10.1146/annurev-earth-040523-021619

Elsner, J. B., & Jagger, T. H. (2008). United States and Caribbean tropical cyclone activity related to the solar cycle. *Geophysical Research Letters*, *35*(18). https://doi.org/10.1029/2008gl034431

Emanuel, K. (2021). Atlantic tropical cyclones downscaled from climate reanalyses show increasing activity over past 150 years. *Nature Communications*, *12*(1), 7027. https://doi.org/10.1038/s41467-021-27364-8

Frappier, A. B. (2013). Masking of interannual climate proxy signals by residual tropical cyclone rainwater: Evidence and challenges for low-latitude speleothem paleoclimatology. *Geochemistry, Geophysics, Geosystems*, *14*(9), 3632–3647. https://doi.org/10.1002/ggge.20218

Garas, K. L., Watanabe, T., & Yamazaki, A. (2023). Hydroclimate seasonality from paired coral Sr/Ca and $\delta^{18}O$ records of Kikai Island, southern Japan: Evidence of East Asian monsoon during the mid-to late Holocene. *Quaternary Science Reviews*, *301*, 107926. https://doi.org/10.1016/j.quascirev.2022.107926

Gori, A., Lin, N., Xi, D., & Emanuel, K. (2022). Tropical cyclone climatology change greatly exacerbates US extreme rainfall–surge hazard. *Nature Climate Change*, *12*(2), 171–178. https://doi.org/10.1038/s41558-021-01272-7

Grossman, E. L., & Ku, T.-L. (1986). Oxygen and carbon isotope fractionation in biogenic aragonite: Temperature effects. *Chemical Geology (Isotope Geoscience Section)*, *59*, 59–74. https://doi.org/10.1016/0168-9622(86)90057-6

Han, Y., Jiang, W., Jiang, L., & Yu, K. (2026). Weakened influence of SST on tropical cyclone frequency during late Holocene warm periods. *Quaternary Science Reviews*, *381*, 109947. https://doi.org/10.1016/j.quascirev.2026.109947

Han, Y. S., Jiang, W., Jiang, L. L., Yong, Y. Y., Yang, K., Gu, T. W., et al. (2024). Corals reveal interdecadal variation of tropical cyclones modulated by Pacific decadal oscillation. *Journal of Geophysical Research-Atmospheres*, *129*(7), e2024JD040824. https://doi.org/10.1029/2024JD040824

Henny, L., Thorncroft, C. D., Hsu, H. H., & Bosart, L. F. (2021). Extreme rainfall in Taiwan: Seasonal statistics and trends. *Journal of Climate*, *34*(12), 4711–4731. https://doi.org/10.1175/Jcli-D-20-0999.1

Hochet, A., Tajouri, S., Kolodziejczyk, N., & Llovel, W. (2025). Mechanisms of tropical sea surface salinity variations at seasonal timescales. *Journal of Geophysical Research: Oceans*, *130*(2), e2024JC021455. https://doi.org/10.1029/2024JC021455

Hu, L., Wen, T., Shao, Y., Wang, Q., Fang, W., Yang, J., et al. (2023). Economic impacts of tropical cyclone-induced multiple hazards in China. *Earth's Future*, *11*(9), e2023EF003622. https://doi.org/10.1029/2023EF003622

Huang, C., Liu, H., Wang, X., Li, H., Zhang, Z., Zuo, J., & Wang, R. (2022). PDO modulation on the relationship between ENSO and typhoon tracks. *Journal of Climate*, *35*(20), 6703–6720. https://doi.org/10.1175/JCLI-D-21-0381.1

Huang, H. P., Collins, W. D., Patricola, C. M., Ruprich-Robert, Y., Ullrich, P. A., & Baker, A. J. (2023). Contrasting responses of Atlantic and Pacific tropical cyclone activity to Atlantic multidecadal variability. *Geophysical Research Letters*, *50*(10), e2023GL102959. https://doi.org/10.1029/2023GL102959

Huang, W. N., & Dong, S. (2019). Long-term and inter-annual variations of tropical cyclones affecting Taiwan region. *Regional Studies in Marine Science*, *30*, 100721. https://doi.org/10.1016/j.rsma.2019.100721

Hung, C. (2013). A 300-year typhoon record in Taiwan and the relationship with solar activity. *Terrestrial, Atmospheric and Oceanic Sciences*, *24*(4 PART II), 737–743. https://doi.org/10.3319/TAO.2013.02.18.01(A)

Huo, W. J., Xiao, Z. N., Wang, X., & Zhao, L. (2021). Lagged responses of the tropical Pacific to the 11-yr solar cycle forcing and possible mechanisms. *Journal of Meteorological Research*, *35*(3), 444–459. https://doi.org/10.1007/s13351-021-0137-8

Huo, W. J., Xiao, Z. N., & Zhao, L. (2023). Phase-Locked impact of the 11-Year solar cycle on tropical Pacific decadal variability. *Journal of Climate*, *36*(2), 421–439. https://doi.org/10.1175/Jcli-D-21-0595.1

Jackisch, D., Yeo, B. X., Switzer, A. D., He, S., Cantarero, D. L. M., Siringan, F. P., & Goodkin, N. F. (2022). Precipitation stable isotopic signatures of tropical cyclones in Metropolitan Manila, Philippines, show significant negative isotopic excursions. *Natural Hazards and Earth System Sciences*, *22*(1), 213–226. https://doi.org/10.5194/nhess-22-213-2022

Jiang, L., & Li, T. (2021). Impacts of tropical North Atlantic and equatorial Atlantic SST anomalies on ENSO. *Journal of Climate*, *34*(14), 5635–5655. https://doi.org/10.1175/JCLI-D-20-0835.1

Jullien, S., Aucan, J., Kestenare, E., Lengaigne, M., & Menkes, C. (2024). Unveiling the global influence of tropical cyclones on extreme waves approaching coastal areas. *Nature Communications*, *15*(1), 6593. https://doi.org/10.1038/s41467-024-50929-2

Kench, P. S., Morgan, K. M., Owen, S. D., Lin, K., Wang, X., & Ramos, R. D. (2025). Coral growth records 20th Century sea-level acceleration and climatic variability in the Indian Ocean. *Nature Communications*, *16*(1), 5872. https://doi.org/10.1038/s41467-025-60972-2

Kilbourne, K. H., Moyer, R. P., Quinn, T. M., & Grottoli, A. G. (2011). Testing coral-based tropical cyclone reconstructions: An example from Puerto Rico. *Palaeogeography, Palaeoclimatology, Palaeoecology*, *307*(1–4), 90–97. https://doi.org/10.1016/j.palaeo.2011.04.027

Kropf, C. M., Vaterlaus, L., Bresch, D. N., & Pellissier, L. (2025). Tropical cyclone risk for global ecosystems in a changing climate. *Nature Climate Change*, *15*(1), 92–100. https://doi.org/10.1038/s41558-024-02194-w

Kumar, M. S., Geethalakshmi, V., Pazhanivelan, S., Subrahmaniyan, K., Dheebakaran, G., Saravanakumar, V., et al. (2025). Tropical cyclone-induced rainfall estimation using the distance approach: A systematic review. *Natural Hazards*, *121*(19), 22297–22339. https://doi.org/10.1007/s11069-025-07689-z

Laurindo, L. C., Siqueira, L., Small, R. J., Thompson, L., & Kirtman, B. P. (2024). Quantifying the contribution of ocean advection and surface flux to the upper-ocean salinity variability resolved by climate model simulations. *Geophysical Research Letters*, *51*(3), e2023GL106354. https://doi.org/10.1029/2023GL106354

Lawman, A. E., Partin, J. W., Dee, S. G., Casadio, C. A., Di Nezio, P., & Quinn, T. M. (2020). Developing a coral proxy system model to compare coral and climate model estimates of changes in paleo-ENSO variability. *Paleoceanography and Paleoclimatology*, *35*(7), e2019PA003836. https://doi.org/10.1029/2019PA003836

Li, D. L., Xiao, Z. N., Xu, J. J., & Zhao, L. (2023). Asymmetric modulation of solar activity on tropical cyclone frequency over the western North Pacific and the possible mechanism. *Frontiers in Earth Science*, *11*, 1169685. https://doi.org/10.3389/feart.2023.1169685

Li, S., Li, Z. Q., & Ling, S. N. (2023). Combined effect of the solar activity and ENSO on the tropical cyclone genesis frequency in the southeastern part of the western North Pacific. *Frontiers in Earth Science*, *11*, 1139699. https://doi.org/10.3389/feart.2023.1139699

Li, S., Xiao, Z., & Zhao, Y. (2023). Modulation of the influence of ENSO on northward-moving tropical cyclones in the Western North Pacific by the North Atlantic tripole SST anomaly pattern. *Journal of Climate*, *36*(2), 405–420. https://doi.org/10.1175/JCLI-D-21-0704.1

Lin, J., Lee, C. Y., Camargo, S. J., Sobel, A. H., & Zhuo, J. Y. (2025). The response of tropical cyclone hazard to natural and forced patterns of warming. *npj Climate and Atmospheric Science*, *8*(1), 109. https://doi.org/10.1038/s41612-025-00997-y

McGregor, S., Timmermann, A., Stuecker, M. F., England, M. H., Merrifield, M., Jin, F.-F., & Chikamoto, Y. (2014). Recent Walker circulation strengthening and Pacific cooling amplified by Atlantic warming. *Nature Climate Change*, *4*(10), 888–892. https://doi.org/10.1038/nclimate2330

Meehl, G. A., Arblaster, J. M., Matthes, K., Sassi, F., & van Loon, H. (2009). Amplifying the Pacific climate system response to a small 11-year solar cycle forcing. *Science*, *325*(5944), 1114–1118. https://doi.org/10.1126/science.1172872

Minamidate, K., & Goto, K. (2024). Unveiling the history and nature of paleostorms in the Holocene. *Earth-Science Reviews*, *253*, 104774. https://doi.org/10.1016/j.earscirev.2024.104774

Misios, S., Gray, L. J., Knudsen, M. F., Karoff, C., Schmidt, H., & Haigh, J. D. (2019). Slowdown of the Walker circulation at solar cycle maximum. *Proceedings of the National Academy of Sciences*, *116*(15), 7186–7191. https://doi.org/10.1073/pnas.1815060116

Monica, S. B., Wallace, D. J., Wallace, E. J., Du, X. J., Dee, S. G., & Anderson, J. B. (2024). 4500-year paleohurricane record from the Western Gulf of Mexico, Coastal Central TX, USA. *Marine Geology*, *473*, 107303. https://doi.org/10.1016/j.margeo.2024.107303

Mueller, T. J., Patricola, C. M., & Bercos-Hickey, E. (2024). The influence of ENSO diversity on future Atlantic tropical cyclone activity. *Journal of Climate*, *37*(15), 3959–3975. https://doi.org/10.1175/Jcli-D-23-0286.1

Pfeiffer, M., Reuning, L., Zinke, J., Garbe-Schönberg, D., Leupold, M., & Dullo, W.-C. (2019). 20th Century $\delta^{18}O$ seawater and salinity variations reconstructed From Paired $\delta^{18}O$ and Sr/Ca Measurements of a La Reunion Coral. *Paleoceanography and Paleoclimatology*, *34*(12), 2183–2200. https://doi.org/10.1029/2019PA003770

Qi, W. Q., Yong, B., Ritchie, E. A., Tyo, J. S., & Toumi, R. (2025). Global increase of tropical cyclone precipitation rate toward coasts. *Geophysical Research Letters*, *52*(17), e2025GL115500. https://doi.org/10.1029/2025GL115500

Qin, L., Zhu, L., Liu, B., Li, Z., Tian, Y., Mitchell, G., et al. (2024). Global expansion of tropical cyclone precipitation footprint. *Nature Communications*, *15*(1), 4824. https://doi.org/10.1038/s41467-024-49115-1

Ramos, R. D. (2020). Houbihu, southern Taiwan *Porites* Sr/Ca and $\delta^{18}O$ data from 1788 to 2013 [Dataset]. *National Oceanic and Atmospheric Administration*. https://www.ncei.noaa.gov/access/paleo-search/study/29412

Ramos, R. D., Goodkin, N. F., & Fan, T. Y. (2020). Coral records at the Northern edge of the Western Pacific warm pool reveal multiple drivers of Sea surface temperature, salinity, and rainfall variability since the end of the little ice Age. *Paleoceanography and Paleoclimatology*, *35*(5), e2019PA003826. https://doi.org/10.1029/2019PA003826

Sánchez-Murillo, R., Durán-Quesada, A. M., Esquivel-Hernández, G., Rojas-Cantillano, D., Birkel, C., Welsh, K., et al. (2019). Deciphering key processes controlling rainfall isotopic variability during extreme tropical cyclones. *Nature Communications*, *10*(1), 4321. https://doi.org/10.1038/s41467-019-12062-3

Scoccimarro, E., Villarini, G., Gualdi, S., & Navarra, A. (2021). The Pacific decadal oscillation modulates tropical cyclone days on the interannual timescale in the North Pacific Ocean. *Journal of Geophysical Research-Atmospheres*, *126*(15), e2021JD034988. https://doi.org/10.1029/2021JD034988

Sena, A., Patricola-DiRosario, C. M., Klotzbach, P., Camargo, S., Lee, C. Y., & Tippett, M. (2025). Multidecadal fluctuations in the observed ENSO-tropical cyclone teleconnection. *Geophysical Research Letters*, *52*(22), e2025GL116968. https://doi.org/10.1029/2025GL116968

Shan, K., Lin, Y., Chu, P. S., Yu, X., & Song, F. (2023). Seasonal advance of intense tropical cyclones in a warming climate. *Nature*, *623*(7985), 83–89. https://doi.org/10.1038/s41586-023-06544-0

Shen, C.-C., Lee, T., Liu, K.-K., Hsu, H.-H., Edwards, R. L., Wang, C.-H., et al. (2005). An evaluation of quantitative reconstruction of past precipitation records using coral skeletal Sr/Ca and $\delta^{18}O$ data. *Earth and Planetary Science Letters*, *237*(3–4), 370–386. https://doi.org/10.1016/j.epsl.2005.06.042

Shi, L., Zhan, R., Zhao, J., & Kug, J. S. (2024). Mutating ENSO impact on Northwest Pacific tropical cyclones under global warming. *Geophysical Research Letters*, *51*(1), e2023GL105864. https://doi.org/10.1029/2023GL105864

Shi, X. M., Liu, Y., Chen, J. N., Chen, H. M., Wang, Y. Y., Lu, Z. M., et al. (2024). Escalating tropical cyclone precipitation extremes and landslide hazards in South China under Global Warming. *npj Climate and Atmospheric Science*, *7*(1), 107. https://doi.org/10.1038/s41612-024-00654-w

Shi, Y., & Jiang, W. (2026). Atlantic multidecadal oscillation and solar forcing modulate decadal-scale variability in Northwest Pacific tropical cyclone precipitation [Dataset]. *Figshare*. https://doi.org/10.6084/m9.figshare.33393436

Shi, Y. P., Zhang, L. Y., & Du, Y. (2025). ENSO modulating tropical cyclone geneses in fall and winter seasons over the South China Sea. *Theoretical and Applied Climatology*, *156*(1), 18. https://doi.org/10.1007/s00704-024-05298-7

Song, J., Klotzbach, P. J., Wei, N., & Duan, Y. (2023). Modulation of western North Pacific tropical cyclone formation by central Pacific El Niño–Southern Oscillation on decadal and interannual timescales. *International Journal of Climatology*, *43*(1), 426–437. https://doi.org/10.1002/joc.7777

Song, K. X., Zhan, R. F., Wang, Y. Q., Zhao, J. W., & Tao, L. (2024). Influence of the Atlantic multidecadal oscillation on the rapid intensification magnitude of tropical cyclones over the Western north Pacific. *Journal of Climate*, *37*(2), 689–703. https://doi.org/10.1175/Jcli-D-23-0131.1

Sun, C., Liu, Y. S., Gong, Z. Q., Kucharski, F., Li, J. P., Wang, Q. Y., & Li, X. (2020). The footprint of Atlantic multidecadal oscillation on the intensity of tropical cyclones over the Western north Pacific. *Frontiers in Earth Science*, *8*, 604807. https://doi.org/10.3389/feart.2020.604807

Sun, C. J., Tian, L. J., Shanahan, T. M., Partin, J. W., Gao, Y. L., Piatrunia, N., & Banner, J. (2022). Isotopic variability in tropical cyclone precipitation is controlled by Rayleigh distillation and cloud microphysics. *Communications Earth and Environment*, *3*(1), 50. https://doi.org/10.1038/s43247-022-00381-1

Sun, J. R., Xu, F. H., Oey, L. Y., & Lin, Y. L. (2019). Monthly variability of Luzon Strait tropical cyclone intensification over the Northern South China Sea in recent decades. *Climate Dynamics*, *52*(5–6), 3631–3642. https://doi.org/10.1007/s00382-018-4341-x

Tao, S., Liu, K.-b., Yan, H., Meng, M., Yu, K., Shi, Q., & Zhang, H. (2024). The history of the El Niño–Southern Oscillation and sea surface salinity during 1376–1500 CE reconstructed by *Porites* coral $\delta^{18}O$ from Huangyan Island, South China Sea. *Global and Planetary Change*, *243*, 104622. https://doi.org/10.1016/j.gloplacha.2024.104622

Thompson, D., Conroy, J., Konecky, B., Stevenson, S., DeLong, K., McKay, N., et al. (2022). Identifying hydro-sensitive coral $\delta^{18}O$ records for improved high-resolution temperature and salinity reconstructions. *Geophysical Research Letters*, *49*(9), e2021GL096153. https://doi.org/10.1029/2021GL096153

Thoppil, P. G. (2025). Sustained freshening of Arabian Sea High Salinity Water induced by extreme precipitation events. *Nature Communications*, *16*(1), 3667. https://doi.org/10.1038/s41467-025-58950-9

Tian, Y., Zhou, W., Zhang, L., Zhang, Y., & Zhang, R. (2023). Changes in ENSO modulation of the distribution of rapidly intensifying tropical cyclones over the Western north Pacific in boreal autumn. *Journal of Climate*, *36*(22), 7739–7753. https://doi.org/10.1175/JCLI-D-23-0084.1

Todorović, S., Wu, H. C., Linsley, B. K., Kuhnert, H., Menkes, C., Isbjakowa, A., & Dissard, D. (2024). Western Pacific warm pool warming and salinity front expansion since 1821 reconstructed from paired Coral $\delta^{18}O$, Sr/Ca, and reconstructed $\delta^{18}Osw$. *Paleoceanography and Paleoclimatology*, *39*(12), e2024PA004843. https://doi.org/10.1029/2024PA004843

Wallace, E. J., Dee, S., Bregy, J., & Emanuel, K. A. (2024). A proxy system modeling approach to combining tree-ring and sediment-based paleotempestological records. *Paleoceanography and Paleoclimatology*, *39*(9), e2024PA004870. https://doi.org/10.1029/2024PA004870

Walter, R. M., Sayani, H. R., Felis, T., Cobb, K. M., Abram, N. J., Arzey, A. K., et al. (2023). The CoralHydro2k database: A global, actively curated compilation of coral $\delta^{18}O$ and Sr / ca proxy records of tropical ocean hydrology and temperature for the Common era. *Earth System Science Data*, *15*(5), 2081–2116. https://doi.org/10.5194/essd-15-2081-2023

Wang, C., Fu, M., Wang, B., Wu, L., & Luo, J. J. (2023). Pacific decadal oscillation modulates the relationship between Pacific Meridional Mode and tropical cyclone genesis in the western North Pacific. *Geophysical Research Letters*, *50*(5), e2022GL101710. https://doi.org/10.1029/2022GL101710

Wang, S., Murakami, H., & Cooke, W. F. (2023). Anthropogenic forcing changes coastal tropical cyclone frequency. *npj Climate and Atmospheric Science*, *6*(1), 187. https://doi.org/10.1038/s41612-023-00516-x

Wu, L., Zhang, H., Chen, J.-M., & Feng, T. (2018). Impact of two types of El Niño on tropical cyclones over the western North Pacific: Sensitivity to location and intensity of Pacific warming. *Journal of Climate*, *31*(5), 1725–1742. https://doi.org/10.1175/JCLI-D-17-0298.1

Wu, Y. S., Ten, H. F., Chan, J. C. L., & Lee, C. S. (2019). Long-term features of tropical cyclones affecting Taiwan. *Terrestrial, Atmospheric and Oceanic Sciences*, *30*(6), 793–802. https://doi.org/10.3319/Tao.2019.04.25.01

Yang, W., Wallace, E., Vecchi, G. A., Donnelly, J. P., Emile-Geay, J., Hakim, G. J., et al. (2024). Last millennium hurricane activity linked to endogenous climate variability. *Nature Communications*, *15*(1), 816. https://doi.org/10.1038/s41467-024-45112-6

Ying, M., Zhang, W., Yu, H., Lu, X. Q., Feng, J. X., Fan, Y. X., et al. (2014). An overview of the China meteorological administration tropical cyclone database. *Journal of Atmospheric and Oceanic Technology*, *31*(2), 287–301. https://doi.org/10.1175/Jtech-D-12-00119.1

Yu, T., Feng, J., Chen, W., & Wang, X. (2021). Persistence and breakdown of the western North Pacific anomalous anticyclone during the EP and CP El Niño decaying spring. *Climate Dynamics*, *57*(11), 3529–3544. https://doi.org/10.1007/s00382-021-05882-x

Zhang, W., Leung, Y., & Fraedrich, K. (2015). Different El Niño types and intense typhoons in the Western North Pacific. *Climate Dynamics*, *44*(11), 2965–2977. https://doi.org/10.1007/s00382-014-2446-4

Zhao, H. K., & Wang, C. Z. (2019). On the relationship between ENSO and tropical cyclones in the western North Pacific during the boreal summer. *Climate Dynamics*, *52*(1–2), 275–288. https://doi.org/10.1007/s00382-018-4136-0

Zhao, J. W., Zhan, R. F., Kim, D., Kug, J. S., Long, J. C., Zhang, L. Y., & Ma, X. F. (2024). Distinct modulations of Northwest Pacific tropical cyclone precipitation by Atlantic multidecadal oscillation and interdecadal Pacific oscillation. *Geophysical Research Letters*, *51*(12), e2023GL107749. https://doi.org/10.1029/2023GL107749

Zhao, N. Y., Yan, H., Shi, G., Luo, F., Han, T., Liu, C. C., & Dodson, J. (2025). Prehistoric shifts in tropical cyclone season in the South China sea: Evidence from daily resolution records of giant clam shells. *npj Climate and Atmospheric Science*, *8*(1), 218. https://doi.org/10.1038/s41612-025-01100-1

Zheng, M., & Wang, C. (2023). Interdecadal changes of tropical cyclone intensity in the South China Sea. *Climate Dynamics*, *60*(1), 409–425. https://doi.org/10.1007/s00382-022-06305-1

Zhou, C., Wu, L. G., Wang, C., & Cao, J. (2024). Shifted relationship between the Pacific decadal oscillation and western North Pacific tropical cyclogenesis since the 1990s. *Environmental Research Letters*, *19*(1), 014071. https://doi.org/10.1088/1748-9326/ad1640

Zhou, W., Leung, L. R., Chang, C.-C., Zhao, M., Hsu, H.-H., Liang, H.-C., et al. (2025). Poleward migration of tropical cyclones over 1980–2024 is dominated by Pacific variability. *Nature Geoscience*, *19*, 1–10. https://doi.org/10.1038/s41561-025-01866-2

References From the Supporting Information

Chen, J.-M., Chen, H.-S., & Liu, J.-S. (2013). Coherent interdecadal variability of tropical cyclone rainfall and seasonal rainfall in Taiwan during October. *Journal of Climate*, *26*(1), 308–321. https://doi.org/10.1175/JCLI-D-11-00697.1

Dang, S., Liu, Z., Yu, K., & Lan, H. (2025). Climate significance of coral-derived seawater $\delta^{18}O$ from the northern South China Sea. *Palaeogeography, Palaeoclimatology, Palaeoecology*, *682*, 113426. https://doi.org/10.1016/j.palaeo.2025.113426

Gagan, M. K., Ayliffe, L. K., Beck, J. W., Cole, J. E., Druffel, E. R. M., Dunbar, R. B., & Schrag, D. P. (2000). New views of tropical paleoclimates from corals. *Quaternary Science Reviews*, *19*(1–5), 45–64. https://doi.org/10.1016/S0277-3791(99)00054-2

Gagan, M. K., Dunbar, G. B., & Suzuki, A. (2012). The effect of skeletal mass accumulation in *Porites* on coral Sr/Ca and $\delta^{18}O$ paleothermometry. *Paleoceanography*, *27*(1). https://doi.org/10.1029/2011PA002215

Guo, H., Chen, X., Guo, Y., Zhao, J.-x., Wei, G., & Deng, W. (2025). Coral-derived seasonal seawater $\delta^{18}O$ records from the Northern South China Sea: Hydroclimatic insights into the medieval climate Anomaly and Little Ice Age. *Global and Planetary Change*, *246*, 104718. https://doi.org/10.1016/j.gloplacha.2025.104718